



Multilayered coating on titanium for controlled release of antimicrobial peptides for the prevention of implant-associated infections



Mehdi Kazemzadeh-Narbat^a, Benjamin F.L. Lai^b, Chuanfan Ding^c, Jayachandran N. Kizhakkedathu^b, Robert E.W. Hancock^d, Rizhi Wang^{a,*}

^a Department of Materials Engineering, University of British Columbia, Vancouver, Canada

^b Department of Pathology and Lab Medicine & Center for Blood Research, University of British Columbia, Vancouver, Canada

^c Department of Chemistry, Fudan University, China

^d Department of Microbiology and Immunology, University of British Columbia, Vancouver, Canada

ARTICLE INFO

Article history:

Received 13 March 2013

Accepted 13 April 2013

Available online 13 May 2013

Keywords:

Antimicrobial peptide

Orthopaedic infections

Titanium

Nanotubes

Calcium phosphate coating

Phospholipid

ABSTRACT

Prevention of bacterial colonization and formation of a bacterial biofilm on implant surfaces has been a challenge in orthopaedic surgery. The treatment of implant-associated infections with conventional antibiotics has become more complicated by the emergence of multi-drug resistant bacteria. Antimicrobial eluting coatings on implants is one of the most promising strategies that have been attempted. This study reports a controlled release of an antimicrobial peptide (AMP) from titanium surface through a non-cytotoxic multilayered coating. Three layers of vertically oriented TiO₂ nanotubes, a thin layer of calcium phosphate coating and a phospholipid (POPC) film were impregnated with a potent broad-spectrum AMP (HHC-36). The coating with controlled and sustained release of AMP was highly effective against both Gram-positive (*Staphylococcus aureus*) and Gram-negative (*Pseudomonas aeruginosa*) bacteria. No cytotoxicity to osteoblast-like cells (MG-63) was observed. Moderate platelet activation and adhesion on the implant surface with no observable activation in solution, and very low red blood cell lysis was observed on the implant. This multi-layer assembly can be a potential approach to locally deliver AMPs to prevent peri-implant infection in orthopaedics without being toxic to host cells.

© 2013 Elsevier Ltd. All rights reserved.

1. Introduction

Titanium and titanium alloys are frequently used in orthopaedic implants because of their good biocompatibility and reliable mechanical properties [1]. However, the formation of a bacterial surface biofilm and compromised immunity at the implant/tissue interface may lead to persistent infections on and around titanium implants. Pathogens such as *Staphylococcus aureus*, *Staphylococcus epidermidis*, and *Pseudomonas aeruginosa* can be acquired shortly after the surgical installation of implants or at a later stage (e.g. via a haematogenous route) [2]. The resulting infection is usually difficult to treat and in most cases, replacement of a prosthesis is the only remedy [3]. Moreover, the emergence of multi-drug resistant bacterium like methicillin-resistant *S. aureus* (MRSA) has critically challenged the use of conventional antibiotics [4]. Systemic administration of antimicrobial agents have several drawbacks such as the relatively low drug concentration at the target site and

potential toxicity [5]. Hence, localized delivery of antimicrobial agents with time-effective handling of infection, while potentially eliminating problems associated with systemic administration, is highly desirable [6,7].

The inhibition of organisms in a complex biofilm requires up to 1000-times the antibiotic dose necessary to combat bacteria in suspension [8]. An ideal local antibiotic release profiles should exhibit a high initial release rate within 6 h post implantation while the immune system is weakened/compromised leaving the implant susceptible to surface bacterial colonization, followed by a continuous 'prophylactic' slow release [8,9]. Conventional antibiotics like vancomycin, tobramycin, and gentamicin have been incorporated in controlled release devices [9]. A serious concern regarding the use of these antibiotics is that the release at levels below the minimal inhibitory concentration (MIC) is likely to evoke bacterial resistance [10]. High doses of antibiotics often generate cell toxicity and may impair osteogenic activity [11]. A promising alternative to conventional antibiotics is the short cationic antimicrobial peptides (AMPs) [12]. AMPs have broad-spectrum antimicrobial activity against Gram-positive and Gram-negative bacteria, and are also known to be antifungal and antiviral [13]. Due to the complex

* Corresponding author. Department of Materials Engineering, University of British Columbia, 309-6350 Stores Road Vancouver, BC V6T 1Z4, Canada.

E-mail address: rzwang@mail.ubc.ca (R. Wang).

mechanisms of AMPs bacteria are killed more rapidly than with conventional antibiotics and it is extremely difficult for bacteria to develop resistance [14,15].

Calcium phosphate coatings and vertically aligned titania nanotubes (NT) are two platforms used for delivering drugs from orthopaedic implants [16,17]. In our previous work, we successfully examined, *in vitro* and *in vivo*, the feasibility of using micro-porous CaP [18,19], and self-organized and vertically oriented TiO₂ nanotubes coatings [20] on Ti surfaces as carriers to deliver peptide HHC-36, one of the most potent broad-spectrum AMPs. Both strategies led to an initial burst release of HHC-36. And HHC-36 onto loaded CaP coated Ti showed no bone growth inhibition. However, the release rate in both systems was too fast, limiting the antimicrobial effects to early stage peri-implant infection [18–20]. The main objective of this study was to develop a layer-by-layer assembly of multi-layer thin films in order to encourage prolonged AMP release on Ti implants. To create a coating that had dual beneficial effects, i.e. antimicrobial and osteoconductive, thin layers of titania NT and CaP coatings were impregnated with AMPs. These films were topped with a thin phospholipid (POPC, palmitoyl-oleoyl phosphatidyl-choline) film to control the release of AMP based on a bio-inspired cell membrane [21,22]. POPC is found naturally in eukaryotic cell membranes and offers the least support for bacteria growth (81% reduction), and the most suitable platform for bone cell attachment [23]. POPC has also been shown to exhibit clinically acceptable osteointegration [24].

Testing of the biocompatibility of coatings has generally been performed through *in vitro* assessment of the interaction of the coatings with recognized cell culture lines. However, this does not adequately address the acceptability of these materials in the blood interfacing environment, which consists of a fibrin film containing platelets and red blood cells and plays a significant role in osteogenesis [25,26]. In this regard, platelet adhesion and activation on an implant surface and the surrounding fluid are critical steps in initiating osteoconduction [27,28]. Therefore, it was also the purpose of this study to address the hemocompatibility of the multi-layer coating systems, using platelet adhesion, activation, and haemolysis studies.

2. Materials and methods

2.1. Fabrication of TiO₂ nanotubes on titanium surface

The commercially pure Ti foils (0.1 mm, 99.6% purity, Goodfellow) were consecutively sonicated in acetone, ethanol, and distilled water and then air dried. Titania nanotubes were prepared using anodization technique, in which Ti was used as the working electrode (anode), and platinum as the cathode. The TiO₂ nanotubes were prepared in 75% glycerol (C₃H₈O₃, Fisher Scientific, Canada) solution containing 0.27 M ammonium fluoride (NH₄F, Fisher Scientific, Canada) at 30 V (DC power supply, Matsusada R4K-80 Series) for 6 h at room temperature. After anodizing, the samples were rinsed with water, and sequentially soaked in absolute ethanol and distilled water overnight and air dried. The nanotube samples were then annealed at 400 °C (5 °C/min) for 3 h and then gradually cooled down in the furnace to crystallize the amorphous TiO₂ nanotubes into the anatase structure, following the protocol of Macak et al. [29].

The antimicrobial peptide HHC-36 (KRWWKWWRR-NH₂) (CPC Scientific, Sunnysvale, CA), was used in our study [30]. To load the HHC-36 into NT specimens (1 × 1 cm), the AMP was dissolved in low surface tension solvent (ethanol), and forced into NT using vacuum-assisted physical adsorption method. Fifty microlitre of a 672 μM HHC-36 solution was pipetted onto the nanotube surfaces, gently spread, and allowed to dry under vacuum desiccator at room temperature for 30 min. The loading process was repeated three times.

2.2. Processing of CaP on TiO₂ nanotubes

Calcium phosphate coating was prepared on titania nanotubes using the drop-and-dry technique, a modified approach of the evaporation-induced surface crystallization technique developed by Duan et al. [31]. The supersaturated calcium phosphate (SSCP) containing 2.32 mM NH₄H₂PO₄ (Fluka), 3.87 mM CaCl₂ (Fluka), 150 mM NaCl (Fluka), 40 mM HCl (Fisher), and 50 mM tris(hydroxymethyl)

aminomethane (Tris) (Fluka) was adjusted to pH 7.30 at room temperature with NaOH (Fisher). Fifty μL of SSCP solution was pipetted onto the specimen surfaces, gently spread, and dried in air at room temperature for 3 h. After repeating the drop-and-dry treatment four times, the samples were each rinsed with PBS and allowed to dry in air. The CaP coated specimens were loaded with AMP by pipetting fifty microlitre of 672 μM HHC-36 solution in ethanol onto the CaP surfaces, and air dried. The loading process was repeated three times.

2.3. Phospholipid coating on CaP

POPC (1-Palmitoyl-2-oleoyl-sn-glycero-3-phosphocholine) (Genzyme Pharmaceuticals) and AMP were dissolved in an appropriate volume of ethanol by sonication to give final concentrations of 26 mM POPC, including 672 μM HHC-36. Fifty μL of this solution (POPC-20) were pipetted onto the specimen surfaces, and dried in air at room temperature. The samples were kept at 4 °C for future experiments.

2.4. Surface characterization

Surface morphologies of the coatings were studied, after being sputter coated with a thin layer of gold, with a field emission scanning electron microscope (FE-SEM Zeiss Sigma) equipped with an energy dispersive X-ray analysis unit (EDS). A focused ion beam (FIB-SEM) analysis was performed using a FEI Helios 650 dual beam microscope to investigate the cross section of specimens. The analysis was carried out at low beam current of 0.20 nA, while the energy of ions was 3 kV. Chemical compositions of coatings were evaluated using EDS, and attenuated total reflectance-Fourier transform infrared spectroscopy (ATR-FTIR Perkin Elmer Spectrum 100) in the range from 4000 to 400 cm⁻¹. Chemical binding between POPC and the peptide in the POPC-20 solution was investigated using liquid chromatography-mass spectrometry (BrukerEsquire-LC/MS). The POPC-20 solution was diluted by ten-fold (HHC-36/POPC:67 μM/2.6 mM in ethanol) and injected at 10 μL/min infusion rate. The *m/z* values were obtained from a mass spectrum average. The mass spectrometer was calibrated using pure POPC and HHC-36 standards.

The wettability of surfaces was characterized by measuring contact angles by the sessile drop method in 1 μL distilled water at room temperature. Images were captured and analysed using Northern Eclipse software at 10× magnification.

2.5. Release profile of AMP

The *in vitro* AMP release kinetics of the samples were measured using ultraviolet-visible spectroscopy (UV/Vis) by recording the absorption peak at 280 nm, which is the characteristic excitation wavelength for tryptophan [32]. Three specimens, nanotube coated Ti loaded with AMP (NT), CaP coated nanotubes loaded with AMP (CaP), and POPC-20 were gently rinsed with PBS and dried at room temperature. The specimens, assessed in triplicate, were then immersed in 1 mL of PBS (pH 7.4) in a glass vial while rotating at 37 °C. All samples were rinsed with PBS. After 30 min, 90 min, 150 min, 270 min, 1 day, 2 day, 3 day, 5 day and 7 day, 500 μL of solution was sampled and fresh PBS was replenished each time samples were taken. The samples were stored at -20 °C, and AMP content was analysed using a UV/Vis to assess the AMP cumulative release ratio. A series of standards in the concentration range of 2–100 μg/mL of HHC-36 in PBS were prepared in triplicate to calibrate the system. AMP quantification was then calculated based on the external standard method. Degradation of POPC-20 samples in 1 mL of PBS (pH 7.4) in a glass vial while rotating at 37 °C were studied in triplicate for up to 7 days. After each day, the samples were fixed in 2.5% glutaraldehyde in PBS for 2 h at 4 °C, dehydrated with graded ethanol (50, 70, 80, 90, 95, and 100%, 15 min each), and examined using an FE-SEM.

2.6. Antimicrobial activity

The assessment of antibacterial activity against both Gram-positive (*S. aureus* ATCC 25293) and Gram-negative (*P. aeruginosa* H1001: lux-CDABE) bacteria was performed by the disk-diffusion assay (Kirby-Bauer). To obtain bacteria in the mid logarithmic phase of growth, 100 μL of an overnight culture of bacteria was transferred into sterile tubes containing 5 mL of MHB and incubated at 37 °C for 1 h. *P. aeruginosa* and *S. aureus* bacterial suspensions were then re-suspended in MHB, to provide a final density of ~10⁶ CFU mL⁻¹. The bacterial suspension (1 mL) was applied uniformly to the surface of a nutrient MH agar plate before placing the disks on the plate. The inoculated agar plates were allowed to dry for 10 min, and then the round disks (1 cm in diameter) of specimens and Ti as negative control, were placed on the inoculated agar, with the coated side touching the inoculated agar. The agar plates were then incubated at 37 °C for 24 h.

The antimicrobial activity of POPC samples was also confirmed by SEM imaging of samples incubated with ~10⁶ CFU mL⁻¹ of *S. aureus* or *P. aeruginosa* overnight at 37 °C. The nanotube sample without AMP treatment was used as control.

2.7. Cell study

Commercially available MG-63 human osteoblast-like cells (ATCC CRL-1427, USA) were cultured in a medium consisting of Dulbecco's Modified Eagle's

Medium (DMEM, GIBCO), including a minimal essential medium supplemented with 10% fetal bovine serum (FBS), and 1% nonessential amino acids (GIBCO). The culture medium was refreshed at 2-day intervals and the incubator temperature maintained at 37 °C under 95% humidified atmosphere with 5% CO₂. Cells were washed with 0.1 M PBS and isolated from culture dishes by trypsinization, and viable cell numbers were checked using the Trypan blue dye exclusion test.

The cytocompatibility levels for cells cultured on specimens was evaluated by measuring the mitochondrial dehydrogenase activity using a modified MTT (3-(4,5-dimethyl-2-tiazolyl)-2,5-diphenyl-2H-tetrazolium bromide) (Biotium) reduction assay. To assess the cytotoxicity of specimens, 10⁴ dispersed cells were seeded in triplicate onto nanotube coated Ti without AMP (NT) or POPC-20. Negative controls were assigned to cells cultured in fresh medium, and normal conditions with no AMP. The cells were allowed to attach for 2 h before adding 1 mL culture medium. Fresh medium was replaced every 2 days and the MTT reduction assay was carried out after 1, 2, and 5 days. After each time point, the media was removed, and 100 µL MTT dissolved in 1 mL serum free medium was added to each well, and wells were incubated for 4 h at 23 °C. Subsequently, the solution was removed and was replaced with 200 µL DMSO (dimethylsulfoxide) to dissolve the resulting reduced product that indicated metabolically active cells. After shaking the plates for 15 min, the absorbance was measured at 570 nm on an ELISA microplate reader (Bio-Tek Instruments).

To study cell attachment, 10⁴ dispersed MG-63 cells were cultured on each sample, and incubated for 4 h. The samples were then washed three times with 0.1 M PBS and incubated in 2.5% glutaraldehyde in PBS for 2 h at 4 °C. After washing the samples 3 times with 0.1 M PBS, specimens were dehydrated using graded ethanol washes (50, 70, 80, 90, 95, and 100%, 15 min each), and critical-point dried (Autosamdri®-815B, Series A). The samples were gold sputter coated (Moorestown, NJ), and viewed using an FE-SEM.

2.8. Platelet activation and adhesion analysis

The collection of blood with approved consent from human volunteers was performed under a protocol approved by the clinical ethics committee of the University of British Columbia. Blood from two healthy donors was collected at the Centre for Blood Research, University of British Columbia, into a tube containing 3.8% sodium citrate with a blood/anticoagulant ratio of 9:1. Platelet rich plasma (PRP) was prepared by centrifuging whole blood samples at 900 rpm for 10 min in an Allegra X-22R Centrifuge (Beckman Coulter, Canada).

The level of platelet activation upon interaction with implants was quantified by flow cytometry. Different samples were soaked and incubated with 740 µL of PRP at 37 °C, including NT, CaP coated NT, POPC-20 which had already been interacted with AMP, and POPC coated Ti without AMP as well as pure Ti as controls. After 2 h, aliquots of the incubation mixtures were removed for assessment of the platelet activation state. Five-µL of post-incubation platelet rich plasma, diluted in 45 µL of HEPES (4-(2-hydroxyethyl)-1-piperazineethanesulfonic acid) buffer, was incubated for 20 min in the dark with 5 µL of monoclonal antibody anti-CD62P-PE (Immunotech). The samples were then stopped by the addition of 0.3 mL of phosphate-buffered saline solution. The level of platelet activation was analysed in a BD FACSCanto II flow cytometer (Becton Dickinson) by gating platelets specific events based on their light scattering profile. The activation of platelets was expressed as the percentage of platelet activation marker CD62P-PE fluorescence detected in the 10,000 total events counted per sample. Duplicate measurements were performed, the mean fluorescence was reported. Treatment with 1 U/mL of bovine thrombin (Sigma) was used as a positive control, and with HEPES buffer as a negative control in this flow cytometric analysis. The samples were also washed with PBS and fixed with 2.5% glutaraldehyde in PBS. After washing the samples with PBS, specimens were dehydrated using graded ethanol (50, 70, 80, 90, 95 and 100%, 15 min each). The samples were gold sputter coated (Moorestown, NJ), and examined using an FE-SEM for platelet adhesion onto each sample surface.

2.9. Red blood cell (RBC) haemolysis assay

In RBC haemolysis study, the same groups of samples as platelet activation analysis were soaked and incubated with 740 µL of 10% haematocrit RBC suspension for 1 h at 37 °C. The 100% lysis of RBCs incubated with distilled H₂O was used as positive control. The percent of RBC lysis was measured by the Drabkin method. Twenty microlitres of the 10% haematocrit RBC suspension mixture was added to 1 mL of Drabkin's solution. The RBC suspension was then centrifuged at 8000 rpm for 3 min, and two hundred microlitres of supernatant solution was also subjected to 1 mL of Drabkin's solution dilution. The difference in optical density (OD) was measured using the spectrophotometer at 540 nm. The percentage of red blood cell lysis (haemolysis degree) in each sample is measured from the OD of supernatant divided the OD of suspension solution.

2.10. Statistical analyses

"Primer of Biostatistics" software was used to calculate the difference between sets of data based on analysis of variance (ANOVA). The *p* value of less than 0.05 was considered statistically significant.

3. Results

3.1. Characteristics of TiO₂ nanotubes

The morphology of titania nanotubes after annealing is shown in Fig. 1a. The FE-SEM images show that titania nanotubes were about 2 µm long with a pore size of approximately 120 nm in diameter with

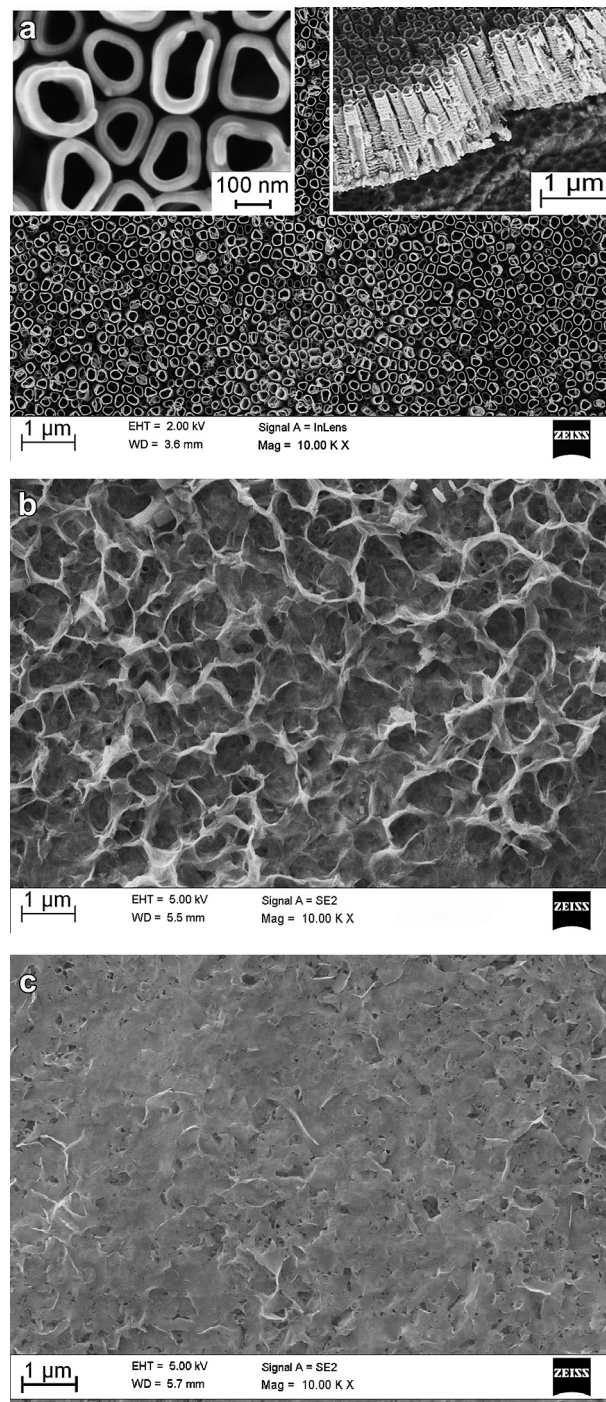


Fig. 1. (a) SEM micrographs of TiO₂ nanotubes including top view, with high magnification showing a close packed structure, and side view of mechanically fractured sample anodized in 75% glycerol solution containing 0.27 M ammonium fluoride at 30 V for 6 h at room temperature. (b) SEM micrograph of CaP coating on TiO₂ nanotubes after four times of drop-and-dry treatment, showing the coverage of NT by CaP crystal flakes. (c) SEM micrograph of POPC-20 coating on CaP.

pores oriented vertically to the sample surface. The nanotube array was uniformly distributed over the substrate. There were ripples observed on the side wall of the nanotubes due to thickness fluctuations along the nanotubes. This phenomenon is related to periodic oscillations of the current during anodization [29].

3.2. Calcium phosphate coating on titania nanotubes surface

Fig. 1b shows the titania nanotube surface treated by the drop-and-dry technique. After four consecutive treatments with the supersaturated calcium phosphate (SSCP) solution, the nanotubes were completely covered with calcium phosphate (CaP) flakes that were about 1 μm large and less than 100 nm in coating thickness based on FIB-SEM analysis. The calcium to phosphorus atomic ratios, as measured by EDS, was calculated to be 1.31 ± 0.04 ($n = 3$), which is close to that of octacalcium phosphate ($\text{Ca/P} = 1.33$). As the layer of CaP was very thin we were unable to perform further analysis with FTIR or XRD.

3.3. Phospholipid coating

The FE-SEM analysis of POPC coated samples showed that the CaP coating was embedded uniformly with POPC all over the sample. POPC filled up the CaP pores but did not completely cover up the CaP coating, so the CaP layer underneath could still be observed (Fig. 1c). The CaP-POPC coating was 200–300 nm thick as observed by FIB-SEM on the multi-layer coated NT. The FTIR spectra of the coatings are shown in Fig. 2a. The assignments corresponding to POPC included the CH_2 antisymmetric stretch and the CH_2

symmetric stretch at 2923 and 2853 cm^{-1} , respectively. The $\text{C}=\text{O}$ stretching vibration band of POPC was observed at about 1735 cm^{-1} . The wave numbers 1463 and 1231 cm^{-1} were attributed to CH_2 scissoring, and the PO_2^- antisymmetric stretch. The 1030–1090 cm^{-1} range included the PO_2^- symmetric stretch, and the $\text{CO}-\text{O}-\text{CH}_2$ symmetric stretch [33].

Identification of the molecular species in the POPC-20 solution was based on the m/z value of their monoisotopic H^+ adducts, as detected by MS (Fig. 2b). The range of fragments detected by MS at 760.8 m/z corresponded to the molecular mass of POPC (760.8 g mol^{-1}), and the peak at 1521 m/z showed the characteristic ions generated from POPC dimers (760.8 + 760.8). A small peak at 1125.1 m/z matched the combined molecular masses of POPC and HHC-36 (1488 g mol^{-1}) with two positive ions H^+ adducts $[(1488 + 760 + 2)/2]$ [34,35] (Fig. 2b).

The hydrophilicity evaluations showed that the cleaned Ti surface (control) had a contact angle of around 67° . The other samples exhibited a decrease in contact angle compared to Ti alone. The obtained contact angles for CaP and NT were about 14° and 10° , respectively, and for POPC and POPC-20 the calculated contact angles were in the range of $7 \pm 1^\circ$.

3.4. Release kinetics and coating degradation

Fig. 3 shows the AMP release profiles of POPC-20 and the two controls. As expected a burst release of AMP was observed from both controls during the first few hours after incubation. In contrast, a slow and steady release of AMP was observed from the POPC-20 samples.

Fig. 4 shows the degradation of POPC-20 coatings after three and seven days in PBS. Nanotubes were observable after three days of incubation, however degradation was heterogeneous and different levels of degradation were detected at random spots.

3.5. Cell attachment and cytotoxicity

Upon interaction with cells and assessment of residual metabolic activity using the MTT reduction assay, statistical analysis of variance showed no significant difference ($p > 0.05$) between samples (POPC-20) and controls (cells cultured in fresh medium, and normal conditions with no AMP, and NT coated Ti without AMP treatment) after 1 day ($p = 0.13$), 2 days ($p = 0.37$) or 5 days ($p = 0.24$) (Fig. 5a). This indicated that the layer modification of the Ti did not affect viability or cellular metabolism.

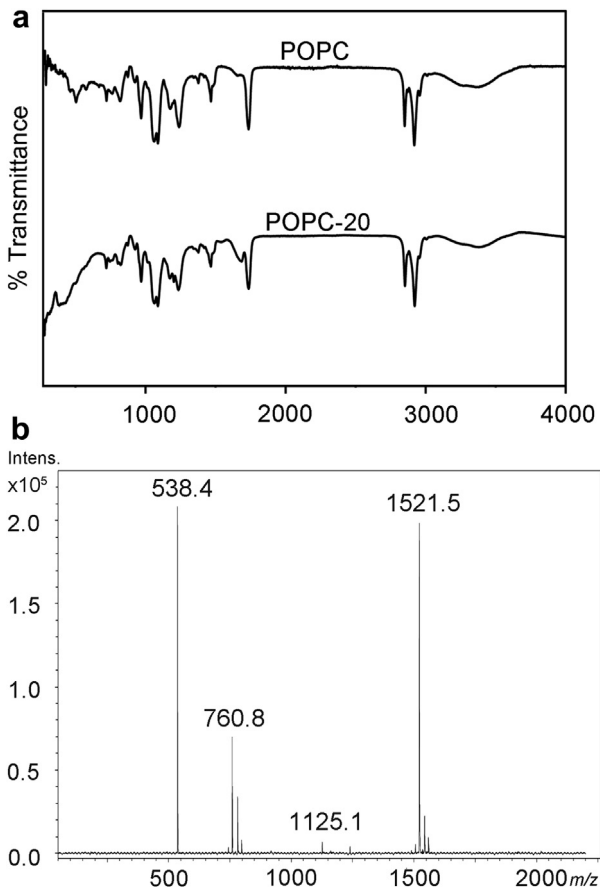


Fig. 2. (a) ATR-FTIR spectra of POPC-20 compare to POPC-only coatings. The inclusion of AMP did not change the chemical characteristics of POPC. (b) Mass spectrum of a ten-fold diluted solution of POPC-20 (HHC-36:POPC of 67 μM :2.6 mM in ethanol).

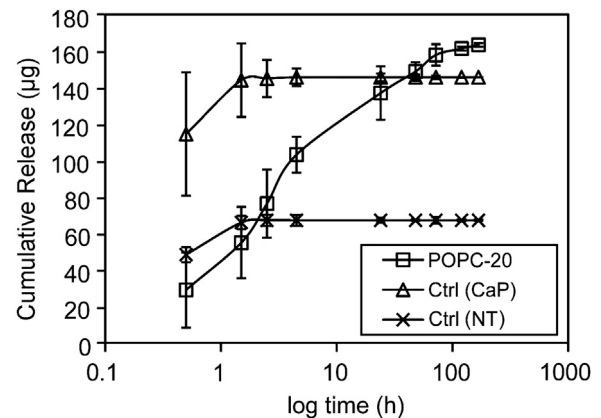


Fig. 3. Kinetics of *in vitro* release of AMP from POPC-20, and NT and CaP controls over time as shown on a log scale. Error bars indicate standard deviations ($n = 4$).

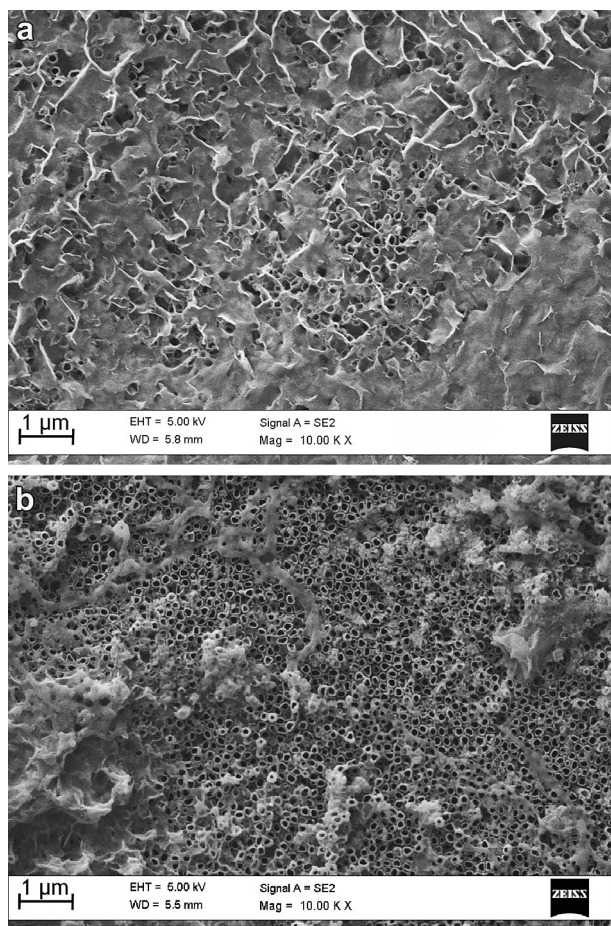


Fig. 4. SEM images of the degradation of POPC-20 after (a) 3 days, and (b) 7 days of incubation in PBS at 37 °C while gently shaking.

After 4 h incubation with 10^4 of MG-63 cells, POPC-20 samples were examined by FE-SEM. Fig. 5b presents typical cell morphologies. The MG-63 osteoblast-like cells spread extensively on substrates. The cells were polygonal in shape with extensive filopodia. However, some thicker cells with elongated appearance were also detected occasionally in random area of samples. In general the cells with a branched look were scattered all over the specimens with no regular orientation. All cells exhibited dorsal ruffles indicating filopodia-mediated events [36,37].

3.6. Antimicrobial activity

The AMP released from the POPC-20 material was able to kill both *S. aureus* and *P. aeruginosa* bacterial strains. A distinct area of clearing around the implants (zone of inhibition) was observed for POPC specimens that had been treated with AMP (Fig. 6).

Fig. 7 shows the qualitative SEM assessment of bacteria incubated with NT controls and POPC-20-coated materials overnight. As expected, the control NT surface showed extensive coverage with bacteria. A self-produced matrix of extracellular polymeric substance from *P. aeruginosa* could be observed in different areas in Fig. 7b of the control NT sample. In strong contrast, very few bacteria were detected on POPC-20 samples, consistent with the observed zone of inhibition (Fig. 6). Evidently, AMP had eluted from the AMP-loaded POPC-20, leading to subsequent bactericidal activity (Fig. 7c,d).

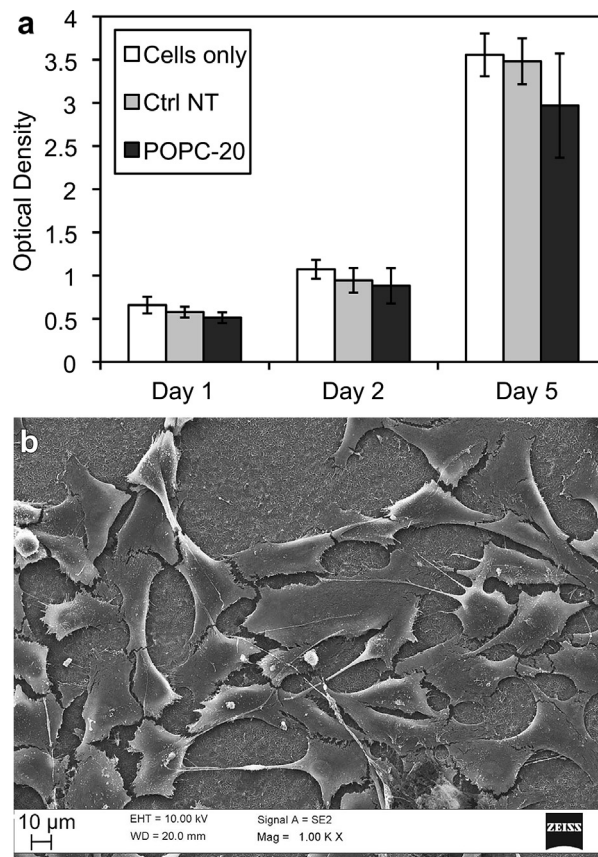


Fig. 5. (a) MTT assay for residual cellular metabolic activity performed to evaluate the cytotoxicity of POPC-20 towards MG-63 osteoblast-like cells. Analysis of variance showed no statistically significant difference ($p > 0.05$) in cell activity between the POPC-20, and two controls (cells only, and NT) after 1 day ($p = 0.13$), 2 days ($p = 0.37$), and 5 days ($p = 0.24$) incubation. (b) SEM photomicrograph of MG-63 osteoblast-like cells on POPC-20 after 4 h of incubation.

3.7. Hemocompatibility

To verify hemocompatibility of the POPC-20, platelet activation and adhesion, and haemolysis in human blood were tested. The percentage of platelets positive for CD62P [38,39] upon interaction with various implant substrates, controls is represented as a chart in Fig. 8. No significant difference ($p > 0.05$) was observed between the levels of platelet activation for POPC-20 and control samples in the solution phase.

The same samples that were used in the platelet activation test were qualitatively examined by FE-SEM analysis for platelet adhesion on POPC-20 samples. Fig. 9 presents typical SEM images of attached platelets after incubation with PRP for 2 h at 37 °C. As shown, platelets adhere to the implant surface. Adhered platelets on all samples showed the presence of pseudopods which are typical for platelets in an activated state [40]. The platelet adhesion appeared to be slightly decreased on POPC-20 than other samples although no statistical analysis could be done. Although, there was not much platelet activation seen in solution, the signs of platelet activation are evident from the platelet adhesion data. This might be due to the small surface area of the implant used in the study (1 cm^2).

As shown in Fig. 10, there was not much haemolysis present on different implant surfaces; it was not statistically different from the PBS control demonstrating that the surface was not lysing RBCs.

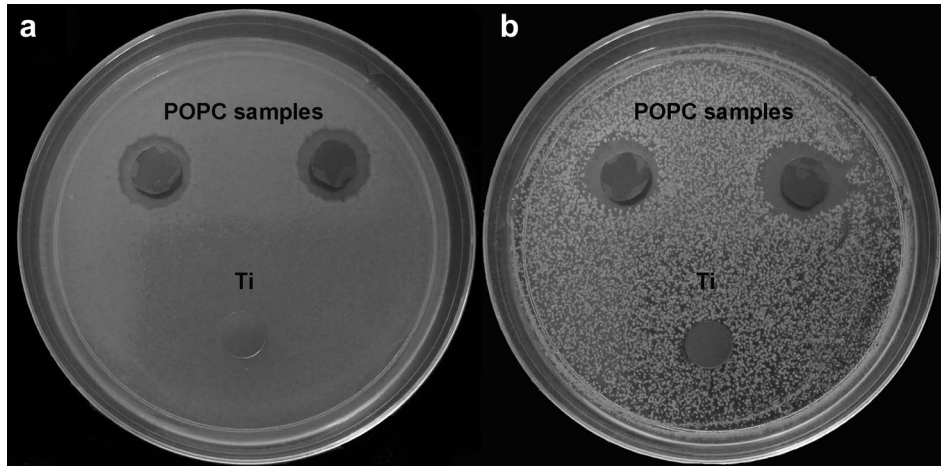


Fig. 6. Evaluation of the antimicrobial effects by the disk-diffusion method against confluent lawns of (a) *P. aeruginosa*, and (b) *Staphylococcus aureus* bacteria. Titanium was used as a control compared to duplicate POPC disks treated with AMP.

4. Discussion

The layer-by-layer technique for flat surfaces is a simple but promising method for coating biological and non-biological substrates impregnated with drugs and other biological substances to enable controlled release [41]. The ideal design of multilayered drug delivery systems as coatings on orthopaedic implants enabling the release of antimicrobial agents in a physiological environment, should meet certain requirements: (1) the selected antimicrobial agents should not promote the development of multiple antibiotic resistance, (2) the release kinetics should be controllable and ideally sustained, and (3) the biocoatings should be osteoconductive.

To achieve these purposes, layer-by-layer coatings on Ti substrates including nanotubes, calcium phosphate and phospholipids

were developed here to enable the delivery of the HHC-36 antimicrobial peptide. HHC-36 has high antimicrobial activities against a broad array of multi-drug-resistant “Superbugs”, including MRSA, and has demonstrated better performance than traditional antibiotics, as well as clinical candidate antimicrobial peptides such as MX226/Omiganan and hLF1-11 [18,42]. The minimal inhibitory concentration (MIC) of HHC-36 is as low as 1.4–2.9 μM against MRSA *S. aureus* and 0.7–5.7 μM against multi-drug resistant *P. aeruginosa* [30,42]. Different models have been proposed for the antimicrobial activity of AMPs, including alterations of membrane-linked functions such as cell wall biosynthesis, cell division and energetics, membrane permeabilization and inhibition of intracellular macromolecular synthesis [12,14,43]. We previously showed that loading HHC-36 antimicrobial peptide into octacalcium phosphate (OCP) coatings and self-organized TiO_2 nanotube arrays

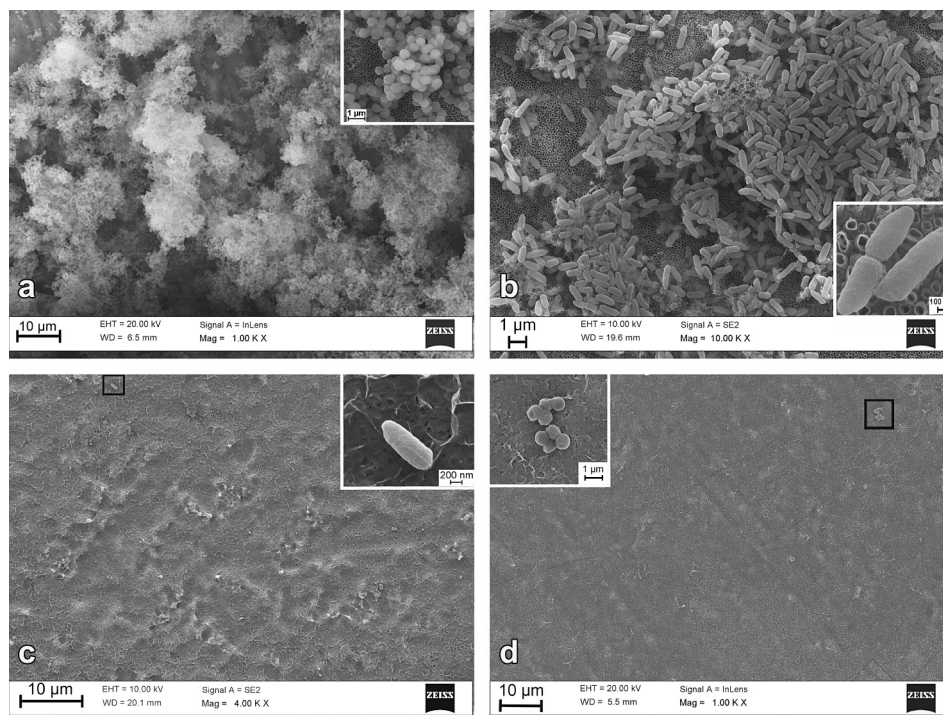


Fig. 7. SEM micrographs of bacteria incubated overnight on the non-AMP treated NT control with (a) *S. aureus*, and (b) *P. aeruginosa* or on the POPC-20 surface with (c) *S. aureus*, and (d) *P. aeruginosa* on. Very few bacteria were observed on the POPC-20 samples.

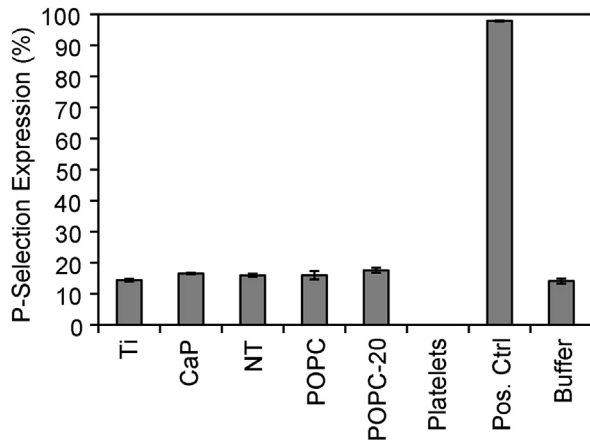


Fig. 8. The percentage of CD62P-selectin expression upon incubation with different samples, showed the lowest platelet activation levels in the fluid phase for all samples. Implant surfaces (1 cm²) were incubated with platelet rich plasma at 37 °C for 2 h and analysis were performed on platelets in solution phase.

did not negatively affect MG-63 osteoblast-like cells [18,20]. The incorporation of HHC-36 into OCP coatings could even moderately enhance bone growth *in vivo* [19].

The drop-and-dry technique developed in this study, enabled the production of different thicknesses of uniform CaP coatings onto TiO₂ nanotubes, ranging from a few nanometres to few microns based on the number of repetitions of coating cycles at low temperature. The suggested mechanism for CaP film formation in the drop-and-dry technique is evaporation-induced surface crystallization [31]. A gradual evaporation of a drop of supersaturated calcium phosphate on a titanium surface would increase the saturation level of CaP and raise the CaP ion concentrations. This would initiate the nucleation of CaP crystals on the surface. The completely dried film would then be like a “crust” layer of CaP and salt crystals (e.g. NaCl, Tris, etc.). By repeating the cycles and rinsing the coating with PBS, the salts would dissolve, and CaP crystals would remain and grow in size and thickness.

To further control the burst release of the incorporated AMP, a thin film of amphiphilic POPC (resembling the lipid bilayer in mammalian cells) was applied as a barrier layer to control the release kinetics. Our current design enabled drug release for up to 72 h using lipid barrier. Mass spectrometry analysis showed much higher signal intensity (Fig. 2b) for POPC compared to the conjugated POPC:HHC-36 peak at 1125 nm, indicating a very weak interaction between these two molecules. This interaction most likely includes hydrogen bonding between tryptophan and cationic residues and POPC (based on [44]) as well as clustering of hydrophobic side chains with the fatty acyl chains of POPC. One of the major advantages to layer-by-layer assembly of multi-layer thin film systems is that the thickness of the films can be tuned by controlling the anodization time of NT, the drop-and-dry cycles of CaP, and the amount and concentration of deposited POPC. Since AMP can be cyclically incorporated throughout each layer, the total drug loading is therefore also (dependently) tuneable.

A first-order model provided the closest fit for the observed release kinetics. Such a model can also be used to describe the drug dissolution of water-soluble drugs in porous matrices or barrier membrane coatings. This means that the system is concentration dependent and we expect the release of AMP occurred via the degradation diffusion phenomenon [45]. Upon contacting PBS in suspensions, the POPC structure would undergo swelling leading to drug diffusion and dissolution. The outermost surface of the POPC layer, representing the diffusion zone, is anticipated to contribute

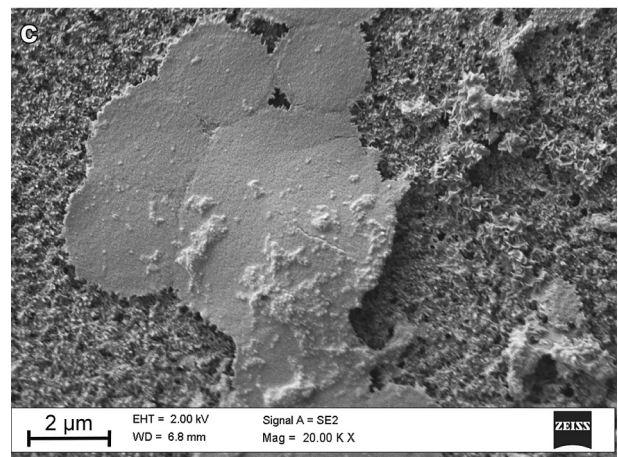
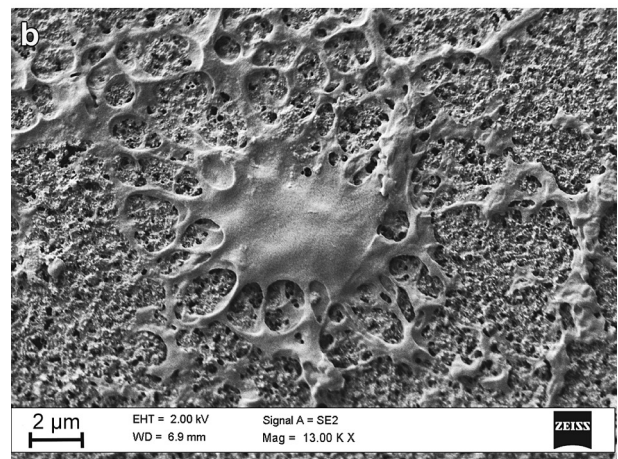
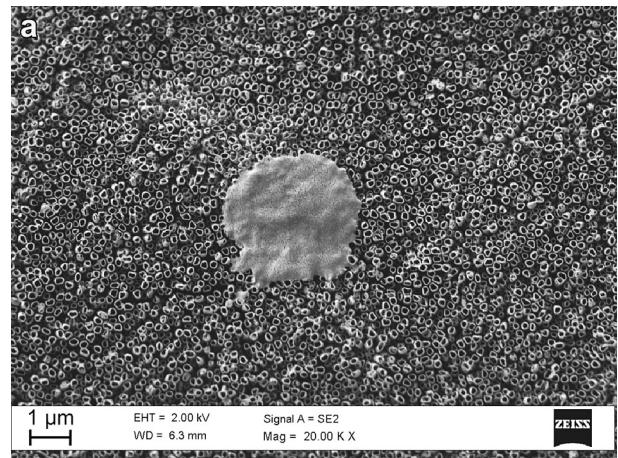


Fig. 9. Platelet adhesion on different implant surfaces characterized by SEM. (a) NT, (b,c) POPC-20 after 2 h incubation with PRP. Activated platelets with pseudopods attached to the coating could be observed on the coating.

most to the initial burst release behaviour of AMP. The heterogeneous degradation pattern of the coatings in Fig. 4 indicates that the POPC layer might swell due to the interaction with PBS during the initial stage, which would eventually lead to the mechanical failure of the coating. However further studies need to be done on the mechanism of release and transition [46].

The established release profile will enable sterilization of the implant site at an early stage and will effectively prevent any surviving bacteria from multiplying and re-colonizing the surface of the implant. Implants exposed to high concentrations of bacteria

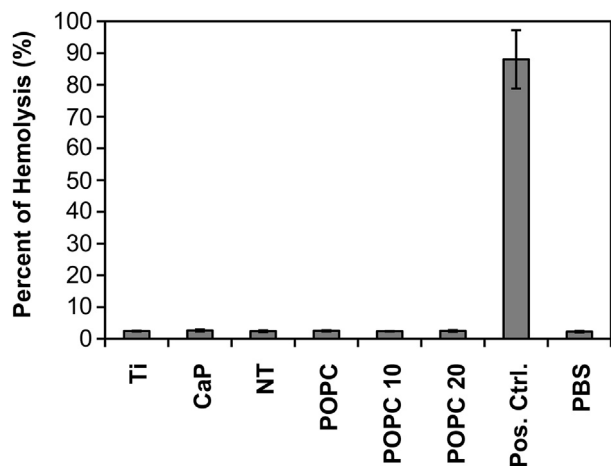


Fig. 10. The haemolytic activity of implants after incubation with 10% haematocrit RBC suspension for 1 h at 37 °C. Very low haemolysis degree was observed for Ti, NT and POCs implant surfaces.

overnight were still effective, indicating the potency in eradicating infection both Gram-positive and Gram-negative bacteria *in vitro* (Figs. 6 and 7). Cytocompatible release levels of HHC-36 (less than 200 μM), together with the low MIC of HHC-36 enables the implants to provide a continuous antimicrobial release while maintaining osteointegration.

The moderate platelet adhesion on hydrophilic implant surfaces, and low platelet activation levels in the fluid phase were observed in the present study (Fig. 8). Other *in vitro* studies have shown favourable cell responses to charged, hydrophilic surfaces, consistent with superior adsorption and bioactivity of adhesion proteins [47,48]. Immediately after implantation, the wound site is first occupied by a blood clot. The initial stage of osteoconduction is the migration of osteogenic cells through a provisional fibrin matrix. Therefore at the first stage of the peri-implant bone healing, both the formation of a fibrin matrix, and the activation of blood cells entrapped at the implant interface, are essential [49]. Upon contact, platelets should undergo the morphological and biochemical changes typically observed in response to foreign surfaces. The changes that have been observed in *in vitro* platelet studies include adhesion, spreading and aggregation [50,51]. Beside platelets, the major cells in the blood that will initially come into contact with the implant surface are the RBCs. It was previously demonstrated that HHC-36 caused minimal red blood cell lysis at concentrations of up to 251 μM [42]. Coatings incorporated with HHC-36 were not damaging red blood cells confirming the non-toxic nature of the substrate.

5. Conclusions

Thin hydrophilic films impregnated with antimicrobial peptide were constructed in layer-by-layer films on titanium implants by creating titania nanotubes, coated with calcium phosphate crystals, and topped with a thin layer of phospholipid. Antimicrobial peptide was loaded into each layer. Utilizing a phospholipid layer as a barrier film enabled more controlled and sustained release of AMP with a first-order model providing the closest fit for the release kinetics. This means that the system was concentration dependent. The films were effective in eradicating the *in vitro* growth of *S. aureus* and *P. aeruginosa* MG-63 osteoblast-like cells attached to the implants and no cytotoxicity was observed after five days. The coatings were degraded heterogeneously and this multi-layer assembly caused moderate platelet activation on the implant surface with no

observable activation in solution. Very low red blood cell lysis was observed on all implants, which further indicated high cytocompatibility. Overall these new layer-by-layer coatings demonstrated excellent functionality.

Acknowledgements

This work was supported by the funding from Natural Sciences and Engineering Research Council of Canada (NSERC) and the Canadian Institutes of Health Research (CIHR). The infrastructure facility at the Centre for Blood Research is supported by the Canada Foundation for Innovation, BCKDF. R.W. is incumbent of the Canada Research Chair in Biomaterials while REWH has a Canada Research Chair in Health and Genomics. JNK is a recipient of a Michael Smith Foundation for Health Research Career Scholar Award. The authors wish to thank Dr. Owen Gethin at Centre for High Throughput Phenogenomics for assisting in FIB-SEM imaging.

Appendix A. Supplementary data

Supplementary data related to this article can be found online at <http://dx.doi.org/10.1016/j.biomaterials.2013.04.036>.

References

- Geetha M, Singh AK, Asokamani R, Gogia AK. Ti based biomaterials, the ultimate choice for orthopaedic implants—a review. *Prog Mater Sci* 2009;54:397–425.
- Costerton JW, Stewart PS, Greenberg EP. Bacterial biofilms: a common cause of persistent infections. *Science* 1999;284:1318–22.
- Darouiche RO. Treatment of infections associated with surgical implants. *N Engl J Med* 2004;350:1422–9.
- Stewart PS, Costerton JW. Antibiotic resistance of bacteria in biofilms. *Lancet* 2001;358:135–8.
- Zhao L, Chu PK, Zhang Y, Wu Z. Antibacterial coatings on titanium implants. *J Biomed Mater Res Part B* 2009;91B:470–80.
- Zilberman M, Elsner JJ. Antibiotic-eluting medical devices for various applications. *J Contr Release* 2008;130:202–15.
- Gao G, Lange D, Hilpert K, Kindrachuk J, Zou Y, Cheng JT, et al. The biocompatibility and biofilm resistance of implant coatings based on hydrophilic polymer brushes conjugated with antimicrobial peptides. *Biomaterials* 2011;32:3899–909.
- Cook J, Griesser HJ, Vasilev K. Antibacterial surfaces for biomedical devices. *Expert Rev Med Devices* 2009;6:553–67.
- Hetrick EM, Schoenfish MH. Reducing implant-related infections: active release strategies. *Chem Soc Rev* 2006;35:780–9.
- Stigter M, Bezemer J, de Groot K, Layrolle P. Incorporation of different antibiotics into carbonated hydroxyapatite coatings on titanium implants, release and antibiotic efficacy. *J Contr Release* 2004;99:127–37.
- Rathbone CR, Cross JD, Brown KV, Murray CK, Wenke JC. Effect of various concentrations of antibiotics on osteogenic cell viability and activity. *J Orthop Res* 2011;29:1070–4.
- Hancock REW, Lehrer R. Cationic peptides: a new source of antibiotics. *Trends Biotechnol* 1998;16:82–8.
- Hancock REW, Diamond G. The role of cationic antimicrobial peptides in innate host defences. *Trends Microbiol* 2000;8:402–10.
- Brogden KA. Antimicrobial peptides: pore formers or metabolic inhibitors in bacteria? *Nat Rev Microbiol* 2005;3:238–50.
- Jensen H, Hamill P, Hancock REW. Peptide antimicrobial agents. *Clin Microbiol Rev* 2006;19:491–511.
- Betty Leon JAJ. Thin calcium phosphate coatings for medical implants. Springer Science; 2009.
- Song Y-Y, Schmidt-Stein F, Bauer S, Schmuki P. Amphiphilic TiO₂ nanotube arrays: an actively controllable drug delivery system. *J Am Chem Soc* 2009;131:4230–2.
- Kazemzadeh-Narbat M, Kindrachuk J, Duan K, Jenssen H, Hancock REW, Wang R. Antimicrobial peptides on calcium phosphate-coated titanium for the prevention of implant-associated infections. *Biomaterials* 2010;31:9519–26.
- Kazemzadeh-Narbat M, Noordin S, Masri BA, Garbuz DS, Duncan CP, Hancock REW, et al. Drug release and bone growth studies of antimicrobial peptide-loaded calcium phosphate coating on titanium. *J Biomed Mater Res Part B: Appl Biomater* 2012;100B:1344–52.
- Ma MH, Kazemzadeh-Narbat M, Hui Y, Lu SS, Ding CF, Chen DDY, et al. Local delivery of antimicrobial peptides using self-organized TiO₂ nanotube arrays for peri-implant infections. *J Biomed Mater Res Part A* 2012;100A:278–85.
- Satsangi A, Satsangi N, Glover R, Satsangi RK, Ong JL. Osteoblast response to phospholipid modified titanium surface. *Biomaterials* 2003;24:4585–9.

- [22] Choi J, Konno T, Takai M, Ishihara K. Regulation of cell proliferation by multi-layered phospholipid polymer hydrogel coatings through controlled release of paclitaxel. *Biomaterials* 2012;33:954–61.
- [23] Willumeit R, Schuster A, Iliev P, Linser S, Feyerabend F. Phospholipids as implant coatings. *J Mater Sci Mater Med* 2007;18:367–80.
- [24] Susin C, Qahash M, Hall J, Sennerby L, Wikesjo UME. Histological and biomechanical evaluation of phosphorylcholine-coated titanium implants. *J Clin Periodontol* 2008;35:270–5.
- [25] Jones MI, McColl IR, Grant DM, Parker KG, Parker TL. Protein adsorption and platelet attachment and activation, on TiN, TiC, and DLC coatings on titanium for cardiovascular applications. *J Biomed Mater Res* 2000;52:413–21.
- [26] Park JY, Davies JE. Red blood cell and platelet interactions with titanium implant surfaces. *Clin Oral Implants Res* 2000;11:530–9.
- [27] Davies JE. In vitro modeling of the bone/implant interface. *Anat Rec* 1996;245:426–45.
- [28] Park JY, Gemmell CH, Davies JE. Platelet interactions with titanium: modulation of platelet activity by surface topography. *Biomaterials* 2001;22:2671–82.
- [29] Macak JM, Schmuki P. Anodic growth of self-organized anodic TiO₂ nanotubes in viscous electrolytes. *Electrochim Acta* 2006;52:1258–64.
- [30] Fjell CD, Jenssen H, Hilpert K, Cheung WA, Pante N, Hancock REW, et al. Identification of novel antibacterial peptides by chemoinformatics and machine learning. *J Med Chem* 2009;52:2006–15.
- [31] Duan K, Tang A, Wang RZ. Accelerating calcium phosphate growth on NaOH-treated poly-(lactic-co-glycolic acid) by evaporation-induced surface crystallization. *Appl Surf Sci* 2008;255:2442–8.
- [32] Pace CN, Vajdos F, Fee L, Grimsley G, Gray T. Hot to measure and predict the molar absorption-coefficient of a protein. *Protein Sci* 1995;4:2411–23.
- [33] Zhao J, Tamm LK. FTIR and fluorescence studies of interactions of synaptic fusion proteins in polymer-supported bilayers. *Langmuir* 2003;19:1838–46.
- [34] Lohmann C, Schachmann E, Dandekar T, Villmann C, Becker CM. Developmental profiling by mass spectrometry of phosphocholine containing phospholipids in the rat nervous system reveals temporo-spatial gradients. *J Neurochem* 2010;114:1119–34.
- [35] Prinz C, Höök F, Malm J, Sjövall P. Structural effects in the analysis of supported lipid bilayers by time-of-flight secondary ion mass spectrometry. *Langmuir* 2007;23:8035–41.
- [36] Davies JE, Causton B, Bovell Y, Davy K, Sturt CS. The migration of osteoblasts over substrata of discrete surface-charge. *Biomaterials* 1986;7:231–3.
- [37] Bohil AB, Robertson BW, Cheney RE. Myosin-X is a molecular motor that functions in filopodia formation. *Proc Natl Acad Sci U S A* 2006;103:12411–6.
- [38] Leytin V, Mody M, Semple JW, Garvey B, Freedman J. Quantification of platelet activation status by analyzing P-selectin expression. *Biochem Biophys Res Commun* 2000;273:565–70.
- [39] Lai BFL, Creagh AL, Janzen J, Haynes CA, Brooks DE, Kizhakkedathu JN. The induction of thrombus generation on nanostructured neutral polymer brush surfaces. *Biomaterials* 2010;31:6710–8.
- [40] Barnhart MI, Walsh RT, Robinson JA. A three-dimensional view of platelet responses to chemical stimuli. *Ann NY Acad Sci* 1972;201:360–90.
- [41] Mansouri S, Winnik FM, Tabrizian M. Modulating the release kinetics through the control of the permeability of the layer-by-layer assembly: a review. *Expert Opin Drug Deliv* 2009;6:585–97.
- [42] Cherkasov A, Hilpert K, Jenssen Hv, Fjell CD, Waldbrook M, Mullaly SC, et al. Use of artificial intelligence in the design of small peptide antibiotics effective against a broad spectrum of highly antibiotic-resistant superbugs. *ACS Chem Biol* 2008;4:65–74.
- [43] Hilpert K, Elliott M, Jenssen H, Kindrachuk J, Fjell CD, Korner J, et al. Screening and characterization of surface-tethered cationic peptides for antimicrobial activity. *Chem Biol* 2009;16:58–69.
- [44] Grossfield A, Woolf TB. Interaction of tryptophan analogs with POPC lipid bilayers investigated by molecular dynamics calculations. *Langmuir* 2002;18:198–210.
- [45] Siepmann J, Siepmann F. Mathematical modeling of drug delivery. *Int J Pharm* 2008;364:328–43.
- [46] Kaunisto E, Marucci M, Borgquist P, Axelsson A. Mechanistic modelling of drug release from polymer-coated and swelling and dissolving polymer matrix systems. *Int J Pharm* 2011;418:54–77.
- [47] Wilson CJ, Clegg RE, Leavesley DI, Pearcy MJ. Mediation of biomaterial-cell interactions by adsorbed proteins: a review. *Tissue Eng* 2005;11:1–18.
- [48] Drinker CK, Drinker KR, Lund CC. The circulation in the mammalian bone-marrow-with especial reference to the factors concerned in the movement of red blood cells from the bone marrow into the circulating blood as disclosed by perfusion of the tibia of the dog and by injections of the bone-marrow in the rabbit and cat. *Am J Physiol* 1922;62:1–92.
- [49] Davies JE. Mechanisms of endosseous integration. *Int J Prosthodont* 1998;11:391–401.
- [50] Shattil SJ, Kashiwagi H, Pampori N. Integrin signaling: the platelet paradigm. *Blood* 1998;91:2645–57.
- [51] Grunkemeier JM, Tsai WB, McFarland CD, Horbett TA. The effect of adsorbed fibrinogen, fibronectin, von willebrand factor and vitronectin on the procoagulant state of adherent platelets. *Biomaterials* 2000;21:2243–52.